Modular Test Bed for Performance Assessment of Piezoelectric Stick-Slip Actuators

D. Pfeffer[1], C. Scholz[2], C. Belly[3], R. Wäsche[2], H.F. Schlaak[1], P.P. Pott[1]
[1] Technische Universität Darmstadt, Darmstadt, Germany
[2] BAM, Bundesanstalt für Materialforschung und -prüfung, Berlin, Germany
[3] CEDRAT Technologies, Meylan Cedex, France

Abstract:
Stepping piezoelectric actuators based on the stick-slip effect inherently make use of a friction contact between stator and rotor. This contact defines not only the actuator's performance but also is prone to wear and tear. For broad use, the actuator has to be able to perform around 1 million strokes. To assess the actuator's performance in terms of force, speed, mechanical output, electrical input, and long-term stability under different load- and environmental conditions, as well as different friction partners, a dedicated test-bed for a LSPA30µXS motor by Cedrat Technologies has been set up.

Keywords: piezoelectric actuator, test bed, stick-slip, performance test, micro positioning

Introduction

Conventional electromagnetic motors are inadequate for many small sized applications, whereas piezoelectric actuators offer good properties such as high power density and large output force.
Piezoelectric stick-slip actuators are widely used in precision positioning applications as lens focal point adjustment, aperture control or small-size robotics. The motion principle is based on the repetitive change between sticking and slipping conditions between stator and rotor/slider (stick-slip motion, see Fig. 1) [1].

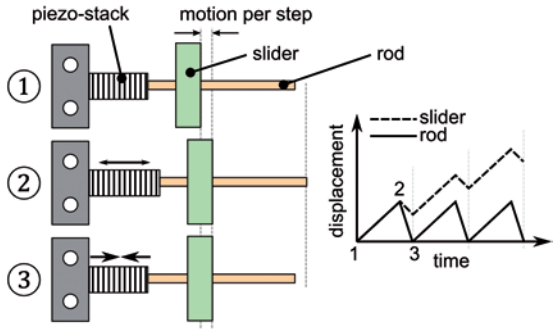

Fig. 1: *Stick-slip actuation principle. 1→2: Slow movement of stator (stick motion). 2→3: Rapid movement of the stator (slip motion). [2]*

The major drawbacks of this actuation principle are wear at the friction contact and parasitic vibration modes.
Both rotational and translational variants of this principle are commonly used for the given applications above, whereas this paper concentrates on linear stepping piezo actuators.
A modular test bed for the detailed investigation of actuation principles and loss mechanisms is proposed. The actuator LSPA30µXS from Cedrat - exemplarily (see Fig. 2).

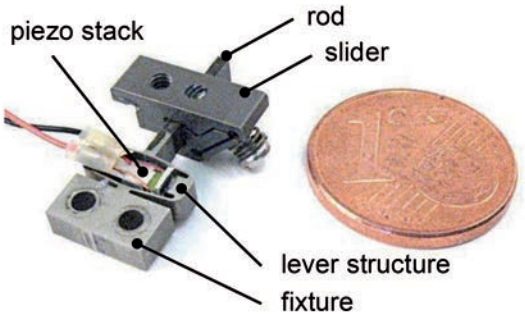

Fig. 2: *Photo of the LSPA30µXS stick-slip actuator (5.6 x 8.8 x 19.15 mm³, mass: 1.9 g).*

The general aims are the verification of the predicted motion of stator and slider, the identification of suitable actuation waveforms and the analysis of loss mechanisms of the examined actuator. In addition, detailed analysis of material combinations of the friction contact will be enabled [3].

Methods

The examination of the wear behavior and loss mechanisms requires the measurement of different mechanical and electrical quantities. Furthermore, qualitative analysis of thermal conditions and parasitic vibration modes are needed to verify model assumptions and/or preceding analytical or finite element simulations. Thus, a set of measurements is defined (see table 1).
The position and velocities shall be measured according to Fig. 3 with respect to the shown x-direction.

Table 1: *Measurands of the test bed*

No.	*Measurement*	*Sym.*	*Unit*
1.a	Macroscopic position of slider	$\bar{x}_s$	mm
1.b	Macroscopic velocity of slider	$\overline{v}_s$	mm/s
1.c	Microscopic velocity of slider	v_s	mm/s
2	Microscopic velocity of rod	v_r	mm/s
3.a	Electrical voltage at piezo stack	$U_{p,RMS}$	V
3.b	Electrical current to piezo stack	$I_{p,RMS}$	mA
3.c	RMS power at piezo stack	P_{RMS}	W
4	Load force	F_{load}	mN
5	Thermal load (IR-picture)	ϑ	°C

It is distinguished between the macroscopic position $\bar{x}_s$ and velocity $\overline{v}_s$ and the microscopic velocities v_s and v_r. While the microscopic velocities give insight into the actual motion of both slider and rod, the macroscopic values show the effective motion of the slider.

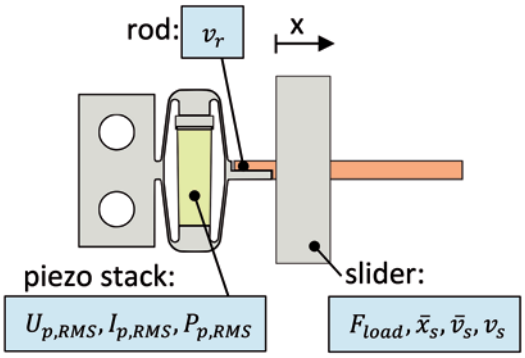

Fig. 3: *Measurement points at the device under test*

The electrical actuation of the piezo stack is of superior interest and has a great influence on efficiency and performance. Both waveform (amplitude as well as shape) and repetition frequency need to be adjustable. The signal needs to be amplified for the piezo stack. Then, voltage and output current of the amplifier are measured and the electrical input power P_{RMS} is obtained by

$$P_{RMS} = U_{p,RMS} \cdot I_{p,RMS} \quad (1)$$

$$P_{RMS} = \sqrt{\overline{(U_p)^2}} \cdot \sqrt{\overline{(I_p)^2}}. \quad (2)$$

The characterization of the actuator will be performed using three different modes of operation:
In mode F (constant force), a defined constant force is applied to the device under test (DUT). This yields the DUTs characteristic curve $\overline{v}_s(F_l)$.
Mode S (constant stiffness) lets the slider run against a spring-like counterpart. This leads to a quick measurement of no-load velocity and blocking force for example while applying different waveforms.
Finally, mode D derives the actuators durability by letting the actuator perform a certain force or velocity profile for a large number of cycles. In this case, the development of characteristic curves and thus the wear behavior can be observed. Occurring debris can be collected and further analyzed.
The measurement process diagram is shown in Fig. 4.

Results

All measurements need to meet the requirements on resolution and range. Table 2 shows all measurement categories with their respective ranges and required resolutions.

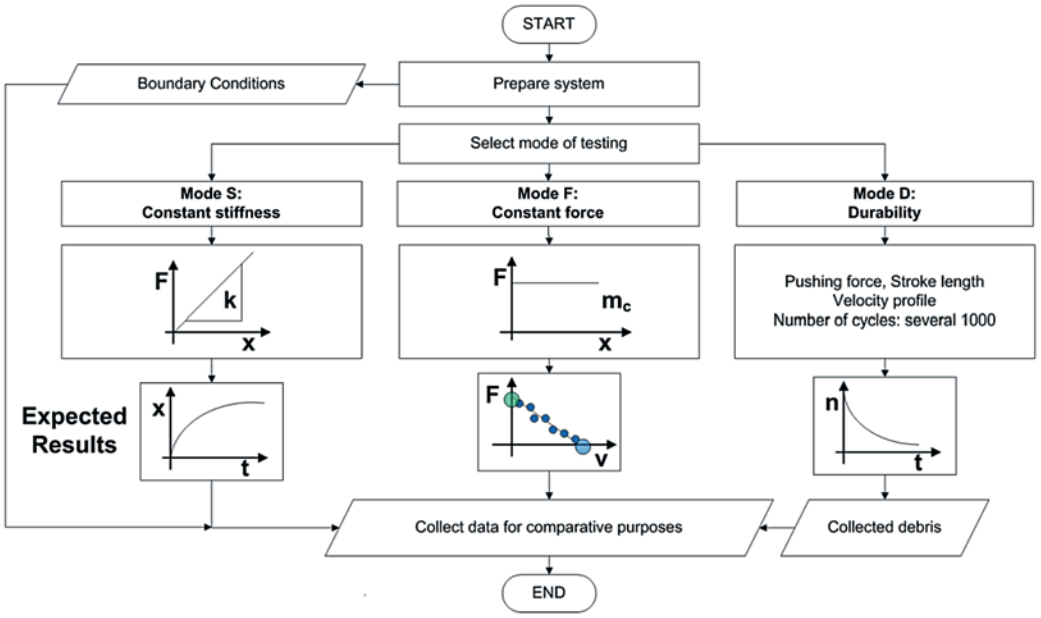

Fig. 4: *Measurement process of the test bed*

Table 2: *Range and precision of the measurands*

No.	*Symbol*	*Range*	*Resolution*	*Unit*
1.a	$\bar{x}_s$	0 to 20	0.02	mm
1.b	$\overline{v}_s$	-100 to 100	1	mm/s
1.c	v_s	-200 to 200	0.1	mm/s
2	v_r	-200 to 200	0.1	mm/s
3.a	$U_{p,RMS}$	0 to 200	0.2	V
3.b	$I_{p,RMS}$	0 to 200	1	mA
4	F_{load}	-1000 to 1000	5	mN
5	ϑ	20 to 80	0.2	°C

All ranges are derived from the nominal data for the exemplary LSPA30µXS actuator.

To avoid unintentional influence on the actuator caused by the measurements it is desired to use contactless measurement principles. Therefore, $\bar{x}_s$ and $\overline{v}_s$ are gathered by a laser triangulator (LK-H052, Keyence, Osaka, JP), at which $\overline{v}_s$ is calculated internally inside the control unit by differentiating the averaged position signal $\bar{x}_s$.

The microscopic velocities v_s and v_r are measured using a two-channel laser vibrometer OVF-2502 (Polytec, Waldbronn, DE). This allows observing the differential velocity by subtracting one signal from the other, which is an indicator for the microscopic relative motion between the friction partners.

Both electrical values $U_{p,RMS}$ and $I_{p,RMS}$ are derived by the LTC1968 IC (Linear Technology, Milpitas, CA, USA) providing a bandwidth of 500 kHz. The analog output values are multiplied using an AD835 IC (Analog Devices, Norwood, MA, USA) to obtain P_{RMS}.

A NI PCI-7830R measurement card with an integrated FPGA in a standard PC is used to gather and digitize $U_{p,RMS}$, $I_{p,RMS}$ and P_{RMS} using the internal 16 bit analog-to-digital converter.

The FPGA on the measurement card generates the arbitrary actuation waveform. This is performed by direct digital synthesis (DDS) technique using a 16 bit look-up table (LUT) with 2048 sampling points. The freely controllable sampling frequency of the DDS allows repetition rates of the waveform of up to 5 kHz. The output range of the digital-to-analog converter is from 0 to 10 V. This voltage is amplified by the factor 20 using a broadband piezo amplifier PDX200D (Piezo Drive, Gilching, DE). The monitor outputs for voltage and current serve as measurement inputs for $U_{p,RMS}$ and $I_{p,RMS}$.

An electrodynamic voice-coil actuator LCA8-010 (SMAC-MCA, Helmond, NL) with a stroke of 10 mm and an integrated linear encoder with 1 µm resolution is used to apply the load force on the DUT. The actual force F_{load} is proportional to the actual current through the excitation coil and can therefore be derived from the actuator control module LCC10.

Using an infrared camera FLIR SC655 (InfraTec, Dresden, DE) the thermal stress of the DUT can be observed. The calibration to the material specific reflection coefficients enables the quantitative measurement of the temperature distribution.

Figure 5 shows the connection diagram of the whole test bed.

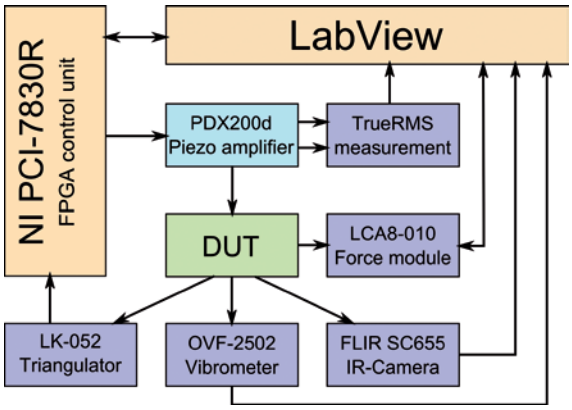

Fig. 5: *Connection diagram of the complete measurement arrangement*

The LUT for the DDS can easily be updated during operation by direct memory access (DMA) to the FPGAs memory from a LabView frontend. The actuation waveform can be chosen from a variety of predefined shapes: saw-tooth, pulse-width modulation (PWM) and exponential (see Fig. 6). It is also allowed to insert a completely free defined LUT from an external data file.

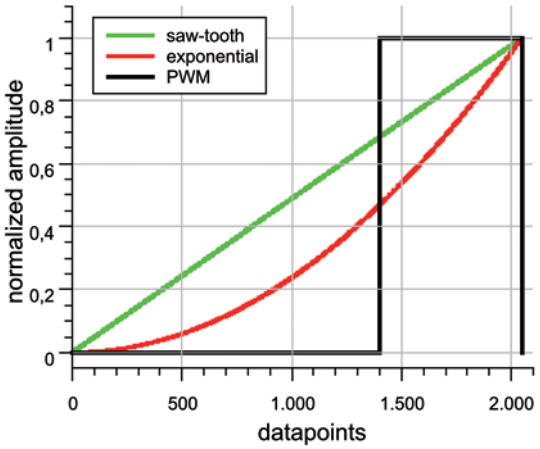

Fig. 6: *Actuation waveform shapes: saw-tooth, exponential, PWM*

The control software of the test bed allows defining the range of motion. To reverse the direction, the actuation waveform is automatically mirrored horizontally. All data is collected simultaneously into a results table. On demand, a given number of cycles of motion can be recorded and divided into

separate curves per cycle. This allows automated statistical analysis of the measurement.

Working Example

Exemplarily the no-load velocity vs. position curve of the LSPA30µXS actuator is evaluated for different waveform amplitudes. A saw-tooth signal with a frequency of 1 kHz is chosen as actuation waveform. The amplitude is swept within the range of 40 to 100 V in 10 V steps.
Figure 7 shows $\overline{v}_s(\bar{x}_s)$ for 15 cycles with a two-sigma band around the mean curve.

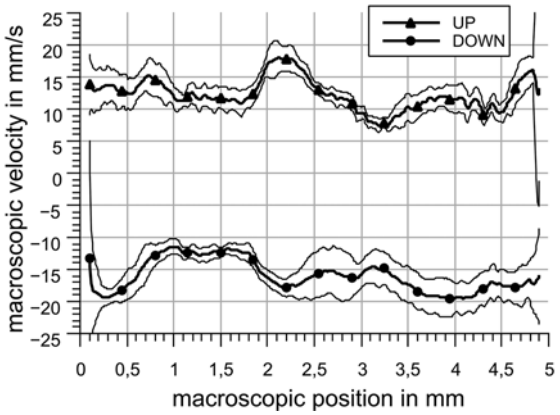

Fig. 7: *Macroscopic velocity of the slider vs. macroscopic position: $\overline{v}_s(\bar{x}_s)$ with no mechanical load. Waveform: 1 kHz saw-tooth at 100 V amplitude. UP: motion towards the tip of the rod; DOWN: motion backwards*

The velocity of the slider with respect to its position on the stator is not constant and lies within an absolute range from 7 to 24 mm/s. The graph shows, that some regions of the rod allow a quicker movement than others. This leads to the conclusion, that either parasitic modal effects interfere with the intended actuation or that the friction contact is not isotropic. The two-sigma band around the mean curves also varies in width from 1.4 to 9 mm/s.
The deviation from a constant macroscopic velocity is similar for different waveform amplitudes (see Fig. 8). Further investigations could address this and improve the consistency of speed along the rod.

Discussion and Outlook

The presented test bed provides a variety of measurements well adapted for LSPA-type motors. An integrated data acquisition system allows the simultaneous observation of the measurands given above.
Some limitations are given through the connection of the counter-force module, as the mechanical impedance is influenced by the mass of the pole. This leads to non-intentional manipulation of the original modes of oscillation. The orientation of the axes of motion is also a crucial factor. Even small deviations from collinearity result in seriously higher friction forces. Finally, the internal linear guidance shows an inherent friction force of approximately 10 mN. Therefore, having the counter-force module connected to the LSPA, it is not possible to perform a no-load measurement.
The slew rate of the used broadband amplifier limits the bandwidth of the output large signal to 14.3 kHz (amplitude: 100 V). However, the small signal bandwidth lies around 200 kHz.
Further improvements of the developed test bed can be related to the analysis of parasitic vibration modes. Concerning this, the additional use of a 2D- or 3D-vibrometer would enhance the observation significantly. Alternatively, a high-speed camera equipped with a macro lens could be used for the same purpose. Furthermore, high-speed imaging can give detailed insight into the actual relative motion at the friction contact.

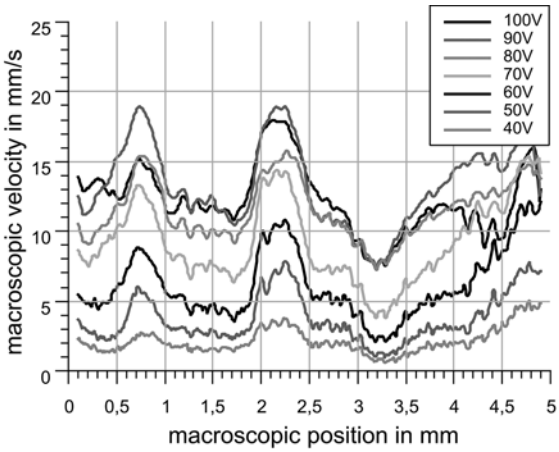

Fig. 8: *$\overline{v}_s(\bar{x}_s)$ for different amplitudes of 1 kHz saw-tooth waveform.*

Acknowledgement

The authors gratefully acknowledge financial support from German Aerospace center (DLR), EUREKA/COST Bureau (Eurostars Project E!6677 NEPIA).

References

[1] C. Belly, Inertial Piezoelectric Motors: Concepts, Projects, Tests and Applications, Dissertation, University of Technology of Belfort Montbéliard, France, 2011
[2] T. Nishimura, T. Morita, Resonant-Type SIDM Actuator, ACTUATOR 2010, Germany, 2010
[3] C. Scholz, R. Wäsche, Stick-Slip and Wear Behaviour of Ceramic and Polymer Materials under Reciprocating Sliding Conditions, World Tribology Congress 2013, Torino, Italy